Devonian-Carboniferous magmatism and glacial sedimentation in Tierra del Fuego, Chile: new evidence from the eastern Cordillera Darwin

***Mauricio Mella[1], David Quiroz[1], Angelina Bustos[2], Luis Yáñez[2]**

[1]*Oficina Regional de Los Lagos, Servicio Nacional de Geología y Minería, La Paz 406, Puerto Varas, Chile. david.quiroz@sernageomin.cl*

[2]*Laboratorio de Geocronología, Servicio Nacional de Geología y Minería, Til-Til 93, Santiago, Chile; angelina.bustos@sernageomin.cl; luis.yanez@sernageomin.cl*

**Contact: mauricio.mella@sernageomin.cl*

ABSTRACT:

The Cordillera Darwin is the highest mountain range in the Fuegian Andes and exposes the oldest rocks of southernmost South America. This study presents new evidence of Devonian magmatism and the sedimentary environment of the late Paleozoic basement identified on the eastern margin of the Cordillera Darwin, specifically the Svea Granite and the Paso Las Lagunas Formation. The findings indicate a crystallization age of ca. 375 Ma for the Svea Granite, constituting the first documented occurrence of Late Devonian peraluminous magmatism in Tierra del Fuego. The granite was subsequently cooled during the latest Devonian, as indicated by a *ca.* 363 Ma $^{40}Ar/^{39}Ar$ muscovite age. The Paso Las Lagunas Formation comprises an approximately 400 m thick succession of immature sedimentary rocks of glacial to periglacial origin. Its depositional age is constrained by U-Pb zircon ages of *ca.* 350 Ma from an andesite intercalated within the upper section of the succession. The overlying sedimentary strata contain a youngest detrital zircon U-Pb age peak at *ca.* 340 Ma, indicating that deposition of the succession continued until at least this time in a periglacial environment. Together with the age of the andesite, the duration of deposition of the Paso Las Lagunas Formation is constrained to at least 10 Myr. These results suggest that the exhumation of the Svea Granite and its country rocks began prior to the deposition of the Paso Las Lagunas Formation. The study provides further support for the hypothesis that the Antarctic Peninsula may have been adjacent to Patagonia during the Devonian. Correlations between the studied rocks and broadly coeval geological units from Patagonia and the Antarctic Peninsula may indicate the existence of a Devonian-Carboniferous magmatic arc between Patagonia and Antarctica.

Keywords: *Paleozoic basement, Svea Granite, Glaciation, Paso Las Lagunas Formation.*

RESUMEN:

La Cordillera Darwin es el cordón montañoso más alto de los Andes fueguinos y expone las rocas más antiguas del extremo austral de América del Sur. Este estudio presenta nuevas evidencias de magmatismo devónico y del ambiente sedimentario del basamento paleozoico tardío identificado en el flanco oriental de la Cordillera Darwin, específicamente el Granito Svea y la Formación Paso Las Lagunas. Los resultados indican una edad de cristalización de ca. 375 Ma para el Granito Svea, lo que constituye la primera evidencia documentada de magmatismo peraluminoso del Devónico Tardío en Tierra del Fuego. Posteriormente, el granito se enfrió durante el Devónico más tardío, como lo indica una edad de *ca.* 363 Ma obtenida mediante $^{40}Ar/^{39}Ar$ en muscovita. La Formación Paso Las Lagunas comprende una sucesión de aproximadamente 400 m de espesor compuesta por rocas sedimentarias inmaduras de origen glaciar a periglaciar. La edad de depositación está acotada por edades U-Pb en circones de *ca.* 350 Ma obtenidas de una andesita intercalada en la sección superior de la sucesión. Las unidades sedimentarias suprayacentes presentan un pico de edad de *ca.* 340 Ma en sus circones detríticos, lo que indica que la depositación de la sucesión continuó hasta al menos ese tiempo en un ambiente periglaciar. En conjunto, estos datos permiten establecer que la depositación de la Formación Paso Las Lagunas se extendió durante al menos 10 millones de años. Estos resultados sugieren que la exhumación del Granito Svea y de sus rocas encajantes comenzó antes de la depositación de la Formación Paso Las Lagunas. Este estudio aporta evidencia adicional a la hipótesis de que la Península Antártica pudo haber estado adyacente a la Patagonia durante el Devónico. Las correlaciones entre las rocas estudiadas y las unidades geológicas aproximadamente coetáneas de la Patagonia y la Península Antártica podrían indicar la existencia de un arco magmático Devónico-Carbonífero entre la Patagonia y la Antártica.

***Palabras clave**: Basamento Paleozoico, Granito Svea, Glaciación, Cordillera Darwin, Tierra del Fuego.*

1. Introduction

The Cordillera Darwin, initially described by Charles Darwin (Darwin, 1846), is a massif located at the southern end of the main island of Tierra del Fuego, between the Beagle Channel and the Seno Almirantazgo fjord in the Fuegian Andes of southernmost South America (Fig. 1). It covers approximately 5,000 km², including the highest mountains (>2000 m a.s.l.) of the Fuegian Andes. Within this massif, metamorphic rocks are grouped into the Cordillera Darwin Metamorphic Complex (CDMC; Cunningham, 1995; Kohn *et al.*, 1995). The CDMC comprises high-grade metamorphic rocks with protoliths ranging in age from the Paleozoic to the Jurassic, which record polyphase deformation (Hervé *et al*., 1979, 1981, 2010a; Nelson, 1982; Kohn *et al*., 1993; Klepeis *et al.,* 2010; Calderón *et al.,* 2021; Betka *et al*., 2022). None of these regional works have documented primary sedimentary structures in the Paleozoic basement of the Cordillera Darwin massif. The objective of this contribution is to characterize the Paleozoic stratigraphic basement units, namely the Svea Granite and the Paso Las Lagunas Formation, recognized on the northeastern flank of the Cordillera Darwin (Fig. 2). Specifically, we aim to describe their lithologies and constrain the timing of crystallization, exhumation and deposition. We further discuss their geodynamic settings and implications for the southwestern margin of Gondwana during the late Paleozoic. This contribution presents the results of fieldwork conducted between 2021 and 2022 by Sernageomin along the northeastern flank of the Cordillera Darwin massif.

2. Geologic and geodynamic setting

In southern Patagonia, the Paleozoic basement comprises several units composed predominantly of metasedimentary rocks with subordinate plutonic bodies. These units have been interpreted as magmatic belts and accretionary complexes (Hervé *et al.*, 2003, 2007a, 2008, 2016; Kohn *et al.*, 1995; Sepúlveda *et al.*, 2008; Calderón *et al.*, 2016; Rojo *et al.*, 2021a, b). In this work, we focus on five of these units: two at the Tierra del Fuego latitude, two farther North (Patagonian Andes and Deseado Massif), and one in the Antarctic Peninsula.

In Tierra del Fuego, the Paleozoic basement is represented by the Tierra del Fuego Igneous Metamorphic Complex (TFIMC; Hervé *et al.*, 2010b) and the CDMC. The TFIMC forms the basement of the Magallanes-Austral Basin (Söllner *et al.*, 2000; Pankhurst *et al.*, 2003; Hervé *et al.*, 2010b), buried beneath thick successions of Meso-Cenozoic sedimentary successions (Hervé *et al.*, 2010b). The TFIMC includes foliated, peraluminous, biotite-bearing granitoids and gneisses, some containing cordierite and garnet; it comprises Cambrian granitoids affected by Permian magmatism and metamorphism (Hervé *et al.*, 2010b; Castillo *et al.*, 2016). The CDMC consists of Paleozoic metasedimentary protoliths, alongside metaplutonic and metavolcanic protoliths of Jurassic-Early Cretaceous age (Barbeau *et al.*, 2009; Hervé *et al.*, 2010a; Cao *et al.*, 2022). These units experienced high- to moderate-grade metamorphism during the closure of the Rocas Verdes marginal back-arc basin during the Late Jurassic-Early Cretaceous, producing a metamorphic zonation defined by biotite, staurolite, kyanite, and sillimanite zones (Nelson *et al.*, 1980; Hervé *et al.*, 1981, 2010a; Kohn *et al.*, 1995; Maloney *et al.*, 2011).

In the southern Patagonian Andes, the Paleozoic basement is represented by the Eastern Andean Metamorphic Complex (EAMC; Hervé *et al.*, 2003). The EAMC comprises two belts: the northeastern EAMC (nEAMC), which includes sedimentary components deposited between the Late Devonian and the early Carboniferous (Augustsson *et al.*, 2006), and is correlated with the Bahia de la Lancha Formation, interpreted as having a glacial origin (Riccardi, 1971; Poiré *et al.*, 1999); and the southwestern EAMC (sEAMC), deposited between the Permian and Triassic (Hervé *et al.*, 2003; Augustsson *et al.*, 2006).

In the eastern sector of the Deseado Massif, plutonic rocks exposed along the Atlantic margin record a protracted history of magmatism from the late Silurian to the early Carboniferous (*ca.* 422, 395, and 346 Ma; Pankhurst *et al.*, 2003; Guido *et al.*, 2005; Ballivián Justiniano *et al.*, 2023). In the western sector of the Deseado Massif, detrital zircon U-Pb data from metasedimentary rocks recovered from boreholes yield a maximum depositional age of 379±4 Ma (Permuy Vidal *et al.*, 2014).

In the Antarctic Peninsula, the basement is represented by the Target Hill Metamorphic Complex consisting of Devonian granitoids and early Carboniferous gneisses (Milne and Millar, 1989). The gneisses have been interpreted as products of partial melting of Devonian granitoids, together representing a Devonian magmatic event and an early Carboniferous metamorphic/magmatic event (Millar *et al.*, 2002; Riley *et al.*, 2023). The recognition of Devonian-Carboniferous tectono-magmatic events in Patagonia and the Antarctic Peninsula suggests these were contiguous magmatic domains along the southwestern Gondwana margin (Pankhurst *et al.*, 2003, 2006; Elliot, 2013; Burton-Johnson and Riley, 2015; Castillo *et al.*, 2017).

Some authors associate the origin of these metamorphic and igneous complexes to the accretionary evolution of the Terra Australis Orogen (*e.g.,* Cawood, 2005; Vaughan and Pankhurst, 2008; Bahlburg, 2022), others with the collision of the Antarctic Peninsula with Patagonia (Devonian-Carboniferous) (*e.g.,* Heredia *et al.*, 2018; Rojo *et al.*, 2021b). Concurrently, enhanced orogenic weathering during the Late Devonian promoted atmospheric CO_2 drawdown, coupled with the establishment of terrestrial forests with deep root systems, contributing to significant paleoclimatic changes that culminated in the Famennian glaciation, characterized by global regressions, narrowing of warm climatic belts, and widespread unconformities (Isaacson *et al.*, 2008).

3. Previous geochronology

The zircon U-Pb ages reported at the TFIMC (Hervé *et al.*, 2010b) display: 1) Cambrian igneous zircons (*ca.* 549-522 Ma); 2) a Cambrian migmatitic gneiss with a late Neoproterozoic peak of inherited igneous zircons; 3) Permian (*ca.* 270 Ma) high-grade metamorphism. The TFIMC shows similar, contemporaneous crustal anatectic processes as the western Antarctic Peninsula in Adie Inlet (cf. Hervé *et al.*, 2010b).

The ages at the CDMC are summarized as follows: 1) U-Pb zircon ages in rhyolitic dykes and deformed granitoids (Darwin suite) at *ca.* 159-97 Ma (Mukasa and Dalziel, 1996; Hervé *et al.*, 2010a; Klepeis *et al.*, 2010); 2) $^{40}Ar/^{39}Ar$ ages in metamorphic muscovite-amphibolite at *ca.* 90-70 Ma (Kohn *et al.*, 1995); 3) U-Pb ages in zircons in pre- and syntectonic granitoids at *ca.* 90-87 Ma (Klepeis *et al.*, 2010); 4) U-Th-Pb ages in S_2 monazite indicate that staurolite and kyanite growth and thus exhumation was underway before 72.6±1.1 Ma (Maloney *et al.*, 2011); 5) U-Pb ages in magmatic zircons in post-deformation granitoids (Beagle suite) at *ca.* 65 Ma (Hervé *et al.*, 1979; Barbeau *et al.*, 2009; Klepeis *et al.*, 2010; Cerredo *et al.*, 2011; González-Guillot *et al.*, 2018; Torres Carbonell *et al.*, 2020; Velásquez *et al.*, 2023); 6) Detrital zircon U-Pb ages in metasedimentary rocks yield younger age peaks, which constrain maximum depositional ages, including: Early Cretaceous (*ca.* 130 Ma), Late Jurassic (*ca.* 160 Ma), Permian (*ca.* 290 Ma), Mississippian (*ca.* 355 Ma) and Devonian (*ca.* 385 and *ca.* 405 Ma) (Barbeau *et al.*, 2009; Hervé *et al.*, 2010a; Cao *et al.*, 2022). This suggests a heterogeneous sedimentary protolith with diverse provenance spanning from the Devonian through the Early Cretaceous.

In the Patagonian Andes, metasediments of the nEAMC show detrital zircon U-Pb age peaks in the range *ca.* 700-350 Ma, with maximum depositional ages at *ca.* 385-350 Ma, *ca.* 330 Ma, and *ca.* 290 Ma (Hervé *et al.*, 2003; Augustsson *et al.*, 2006; Malkowski *et al.*, 2016; Rojo *et al.*, 2021a). The Bahía de la Lancha Formation shows a youngest maximum depositional age of *ca.* 345 Ma (youngest peak; Augustsson *et al.*, 2006).

In the Antarctic Peninsula, the Target Hill Metamorphic Complex comprises orthogneisses and leucogranites with U-Pb ages of *ca.* 398-393 Ma (Devonian) and *ca.* 327 Ma (Mississippian), interpreted as crystallization and metamorphic-magmatic ages, respectively (Millar *et al.*, 2002).

The Lapataia Formation, located closest to the southeast of the study zone in the Argentinian Fuegian Andes, is a low-grade metamorphic unit, with preserved primary structures, interpreted as the basal unit of the Rocas Verdes Basin (Cao *et al.*, 2022; Torres Carbonell *et al.*, 2026). Six samples yielded Paleozoic-age detrital zircons, with maximum depositional ages of *ca.* 267, 349, 355, and 466 Ma. Additional age peaks at *ca.* 540-650 Ma and 990-1000 Ma, some corresponding to inherited zircon grains, indicate contributions from Cambrian and Precambrian to Paleozoic sedimentary sources (Cao *et al.*, 2022; Torres Carbonell *et al.*, 2026).

4. Methodology

Field work, lithological descriptions and sample collection were carried out at several outcrops to outdate the geological map of Mella *et al.* (2025) (Fig. 1). Petrographic thin sections of selected rocks allowed the determination of mineral assemblages and textures. The whole-rock geochemical analyses of a granite (sample MM100320-1Dd) and an andesite (sample MM100320-4Ad) were conducted at the Sernageomin laboratory following the methodology described by Velásquez *et al.* (2023). Three U-Pb ages in magmatic zircons (samples MM100320-1Cd, MM100320-1Dd, and MM100320-4Ad) and six U-Pb ages in detrital zircons (samples TFDQ-19d, MM100320-1Ad, MM060321-2Bd, MM070322-03Dd, TFDQ-14d, and MM130221-4d) were performed by LA-ICP-MS at the Sernageomin laboratory. One U-Pb age in magmatic zircons (sample MM091222-03d) and two U-Pb detrital zircon ages (samples MM091222-02d and MM160223-02d) were performed by LA-ICP-MS at ZirChron LLC, Tucson, Arizona. We handled the data and calculated ages using Isoplot (Ludwig, 2012) and IsoplotR (Vermeesch, 2018). Uncertainties were given as 95% confidence limits (2σ uncertainties) on all calculated weighted mean ages reported in this paper. Two $^{40}Ar/^{39}Ar$ muscovite ages were performed at the Sernageomin laboratory on a muscovite-biotite monzogranite (sample MM100320-1Dd) and a muscovite-bearing orthogneiss (sample MM100320-1Cd). Methodological details and additional analytical data supporting this study are available in Supplementary Material 1 and 2 and Supplementary Tables 1 and 2. Results are shown in Table 1 and figures 3-5.

5. Results

5.1 Field relationships and stratigraphy of Paleozoic stratigraphic basement, northeastern flank of Cordillera Darwin

The Svea Granite (Quensel, 1910), covering an area of approximately 4 km², crops out at Monte Svea (Figs. 1 and 2). It is a monzogranite with a medium- to coarse-grained equigranular texture, comprising muscovite and biotite. The granite constitutes the core of a recumbent mesoscale fold with a north-northeastward vergence (Fig. 1). This folding event is also associated with the development of mylonitic fabrics within the Paso Las Lagunas Formation and Jurassic silicic volcanoclastic successions (Tobífera Formation). On the northern flank of Monte Svea, the granite is unconformably overlain by the Paso Las Lagunas Formation (Fig. 2A, B). This interpretation is supported by 1) erosive fluvial channel contact and load casts indicating inverse polarity between the Svea Granite and the Paso Las Lagunas Formation (Fig. 2B); 2) fluvial arkoses containing clasts and detrital minerals derived from the Svea Granite (see Section 5.3.2 and figure 5); 3) glacial diamictites, containing faceted clasts of the Svea Granite (Fig. 2C, 2C.1). The host rock of the Svea Granite was not observed during fieldwork. On the eastern flank of Monte Svea, an orthogneiss cobble clast, from the present-day end moraine, composed of quartz, orthoclase, muscovite, and chloritized biotite, was analyzed.

The Paso Las Lagunas Formation corresponds to a ~400 m thick succession of immature clastic sedimentary rocks, exposed on the eastern slope of Monte Svea in the Paso Las Lagunas sector, between the Glaciar Marinelli Thrust and the Paso Las Lagunas Thrust (Fig. 1). The succession has a general attitude dipping south-westward (S_0~N115-160°/15-55°), with a protomylonitic fabric with reverse shear-sense indicators (north-eastward vergence) localized along fine-grained layers (S_1~ N130°/20–55°; Figs. 1, 2A and 2C), whereas primary structures remain preserved in poorly deformed domains (Fig. 2B, F).

Two stratigraphic sections were described in detail. At the Paso Las Lagunas sector, the lower (basal) section overlies the Svea Granite across an unconformable contact characterized by inverse stratigraphic polarity (Figs. 1 and 2B). It comprises ~100 m of laminated, medium- to fine-grained arkosic sandstones and quartz sandstones (Figs. 2B and 5), which grade upward into a ~50 m interval of paraconglomerates and orthoconglomerates with minor sandstone intercalations. The upper section comprises ~250 m of pebbly shales grading into pebbly fine-grained sandstones, characterized by a rhythmic alternation of laminated fine-grained wackestone and organic mudstone (diamictite and varves; Fig. 2C, F), with subordinate strata of sandstone, orthoconglomerate and paraconglomerate (Fig. 2D). Load clasts and rhythmic fine-grained wacke sandstone and mudstone are observed. The section is capped by a 3-4 m thick porphyritic andesite (Fig. 2E) whose contacts remain undetermined owing to pervasive brecciation, possibly indicating emplacement as a lava flow; overlying the andesite occur pebbly shales, clast-bearing wackestones, and paraconglomerates.

At Fiordo Parry, an ~100 m thick upper section consists of arkosic sandstones and pebbly shales with intrasparite interbeds showing protomylonitic foliation (S_0~N120°/20°; S_1~145°/15°; Fig. 1). The top of the succession at Paso Las Lagunas and Fiordo Parry is interrupted by a reverse, ~N145°/45° thrust fault (Paso Las Lagunas Thrust), which defines the contact between this unit and the tectonically underlying Tobífera Formation (Fig. 1).

At Monte Svea, the Paso Las Lagunas Formation defines a synformal anticline with the Svea Granite exposed in its core (Figs. 1 and 2A). This geometry requires two superimposed deformation phases, as indicated by several regional studies for the Late Cretaceous in the zone (*e.g.*, Klepeis *et al.*, 2010; Torres Carbonell *et al.*, 2026).

5.2 Petrography

5.2.1 Plutonic rocks (Svea Granite; monzogranite and orthogneiss)

The Svea Granite (Fig. 3A) comprises a medium- to coarse-grained monzogranite composed of quartz, plagioclase, and orthoclase (samples MM100320-1Dd and MM091222-03d; Fig. 2A, B). Orthoclase occurs as large anhedral crystals exhibiting a perthitic texture. Interstitial muscovite (Ms1; ~15% of the total sample) and partially chloritized biotite are also present. Accessory minerals such as apatite, titanite, magnetite, zircon, as well as xenotime and allanite (as inclusions within chloritized biotite) are often present. Secondary minerals, including chlorite, muscovite (Ms2) and fine clay minerals overgrowth orthoclase. Some quartz crystals exhibit textures such as grain boundary migration, bulging, and undulatory extinction, while orthoclase displays diffuse microcline twinning; together, these microstructures suggest low-temperature deformation during the cooling stages of crystallization.

The orthogneiss cobble (Fig. 4A) is a medium to coarse-grained rock showing anisotropic fabric and granoblastic texture (sample MM100320-1Cd). It is composed of elongated quartz (~50%) showing dynamic recrystallization textures (subgrain rotation, bulging, and undulatory extinction), plagioclase (~15%) that is deformed and replaced by sericite, large and deformed orthoclase (~15%) with perthitic textures, muscovite (~10%), and biotite (~10%). Accessory minerals include allanite, titanite, ilmenite, apatite and zircon. Biotite is partially to fully replaced by chlorite and epidote. The foliation is also defined by preferentially oriented laths of muscovite and sericite. The preserved relict mineralogy indicates that the protolith was a muscovite- and biotite-bearing granite.

5.2.2 Sedimentary and volcanic rocks (Paso Las Lagunas Formation)

Arkosic sandstones (samples MM091222-02d and MM130321-4d; Fig. 2B) are laminated, medium- to fine-grained, and well-sorted. They comprise alternating layers containing subangular to angular clasts of quartz (~50%), orthoclase (~40%), and plagioclase (~10%), with quartz and illite cement.

Quartz-rich sandstones (sample TFDQ-19d; Fig. 2A) consist of ~90% quartz grains and display a protomylonitic foliation. They contain subangular to slightly sigmoidal quartz clasts with undulatory extinction (~50%; 0.1-0.5 mm) and larger quartz clasts with undulatory extinction and bulging (~10%; 0.8-2.0 mm), together with orthoclase (~10%), locally altered to illite, and plagioclase (<5%). The microcrystalline matrix (~25%) consists of quartz, illite-chlorite, and muscovite. Accessory minerals include zircon and rutile. Secondary pyrite is also present.

Pebbly shales or diamictites (sample TFDQ-14d; Fig. 2C.1) present ~20% of cobble and pebble clasts consisting of granite, sandstone (sample MM060321-2Bd), shale and limestone dispersed in the matrix (70%, ~0.1 mm). They show alternating bands of sericite, phyllosilicates and microcrystalline quartz (~10%) and plagioclase (~10%) grains partially replaced by sericite-illite. Kerogen and load cast are observed. The protomylonitic foliation is defined by oriented sericite (Fig. 2C).

Wackes (sample MM100320-1Ad; Fig. 2B) are fine-grained rocks consisting of subangular quartz clasts (~55%;), with slight wavy extinction, and subangular lithics (~20%) in a sericite-illite-chlorite matrix (~25%), interstratified with laminated mudstone with kerogen (10%), and iron hydroxide and syntaxial quartz cement. Pyrite and chalcopyrite are also present. Load clasts and rhythmic fine-grained wacke sandstone and mudstone are observed.

The hornblende andesite (sample MM100320-4Ad; Fig. 2D), from the upper section of the Paso Las Lagunas Formation, has a porphyritic texture, with phenocrysts of sericitized plagioclase (20%), euhedral quartz (5%), and chloritized hornblende (5%) set in a groundmass of chlorite and sericite. Accessory minerals include apatite, titanite, magnetite, and zircon. Secondary minerals include epidote, carbonate, chlorite, and sericite.

Limestones (intrasparite; sample MM070322-03Dd) show pebble clasts (20%) of granitoid, andesite, and quartz placed in a matrix (80%) of subangular quartz (30%)

and feldspar (10%) ~30 μm sized surrounded by sparite (60%). This texture is interpreted as indicative of a shallow subaqueous environment with low energy and proximity to the sediment provenance.

Paraconglomerates (sample MM160223-02d) consist of pebble and cobble clasts (60% of 1-10 cm) of granite, gneiss, tuffites, sandstone, and arkosic sandstone, embedded in a matrix (40%) with subangular and angular clasts (<1 mm) of quartz and plagioclase, with sericite, opaque ferric minerals, and subordinate kerogen.

5.3 Geochronology

For U-Pb zircon dating, agreement among independent concordant methods yields the most defensible crystallization ages; concordant zircon and TuffZirc age (Lanphere and Baadsgaard, 2001) estimates establish robust crystallization chronology (Supplementary Table 2). For $^{40}Ar/^{39}Ar$ dating, plateau and inverse isochron ages are reported with concordant MSWD values (Mean Squared Weighted Deviations) interpreted as very good to acceptable (MSWD<2.5-3.0), ensuring age reliability (Supplementary Material 2). This integrated geochronological approach, combining $^{40}Ar/^{39}Ar$ and U-Pb constraints, provides comprehensive and mutually corroborating age determinations.

5.3.1 Svea Granite

The Svea Granite contains a population of euhedral, prismatic zircons that display a normal zoned igneous internal structure and inherited cores, as shown by CL imaging (Fig. 3A). Two U-Pb ages (representative zircon mean) in the monzogranite were concordant at *ca.* 375 Ma (375±2 Ma, MSWD=2.6, sample MM100320-1Dd; 375±1 Ma, MSWD=1.4, sample MM091222-03d) (Fig. 3C; Supplementary Table 2). The orthogneiss cobble (sample MM100320-1Cd) shows a representative zircon mean age of 387±3 Ma (n=5; MSWD=1.5), with a lower intercept age of 387±2 Ma (n=8; MSWD=5) (Fig. 4C; Supplementary Table 2). We interpret these as the crystallization ages of zoned igneous zircon from granite and the zircon core from the igneous protolith of the gneiss, respectively. In addition, two plateau $^{40}Ar/^{39}Ar$ ages, with a concordant inverse isochron age, were obtained in muscovite: 363.4±1.3 Ma (primary muscovite, Ms1, in monzogranite sample MM100320-1Dd; MSWD=0.72 based on 7/8 steps) and 345.5±1.5 Ma (secondary muscovite, Ms2, in orthogneiss cobble sample MM100320-1Cd; MSWD=2.8 based on 6/8 steps) (Figs. 3B and 4B; Supplementary Material 2). We interpret these as cooling (Ms1) and deformation (Ms2) ages, respectively. Consistent with this, both the relative probability plot of $^{206}Pb/^{238}U$ ages and the Tera-Wasserburg diagram show a slight asymmetry toward younger ages, interpreted as reflecting radiogenic Pb loss (Fig. 3C; Supplementary Table 2). Likewise, the younger ages recorded at the outermost rims of some larger zircon grains are interpreted as evidence of incipient Permian metamorphic overgrowth (Fig. 3A).

5.3.2 Paso Las Lagunas Formation

The basal arkosic sandstones have similar detrital zircon age distribution patterns (Fig. 5; Supplementary Table 2). Sample MM091222-02d shows a prominent peak at *ca.* 376 Ma, with a representative zircon mean age of 376±2 Ma (n=8; MSWD=2.9) and a TuffZirc age of 376+1/−4 Ma (n=28, 95% confidence). Sample MM130321-4d likewise shows a major peak at ca. 382 Ma, with a representative zircon mean age of 377±2 Ma (n=10; MSWD=1.9) and a TuffZirc age of 376+4/−3 Ma (n=10, 95% confidence). In both samples, subordinate group of zircon grains (n≤3) falls within the uncertainty of a younger peak at 339±2 Ma and 355±4 Ma, respectively. In the Tera-Wasserburg diagram, these data define an array parallel to the x-axis, at nearly constant $^{207}Pb/^{206}Pb$, interpreted as recent Pb loss and comparable to the Pb-loss trend recorded in the Svea Granite (Figs. 3C and 5).

Detrital zircon age distribution patterns in the sandstone TFDQ-19d display a predominant peak at *ca.* 400 Ma (relative probability from 119 zircon grains); smaller peaks are at *ca.* 570 Ma, *ca.* 740 Ma and *ca.* 1000 Ma, with a single Archaean grain

(Fig. 5; Supplementary Table 2). Four grains with an igneous composition (Th/U>0.2) determine the youngest peak at 372±2 Ma (MSWD=2.2).

The pebbly shales (sample TFDQ-14d) yield a range of detrital zircon ages, with peaks spanning from 375±2 Ma (n=4; MSWD=13; maximum depositional age n≥3) to *ca.* 1000 Ma. The most prominent age peak occurs at *ca.* 570 Ma, with smaller peaks at *ca.* 1300 Ma and *ca.* 1600 Ma, and three Archaean grains (Fig. 5; Supplementary Table 2).

The laminated wacke sandstone MM100320-1Ad shows a more prominent peak at *ca.* 540 Ma, with smaller peaks at *ca.* 350 Ma (younger peak) and *ca.* 1100 Ma (Fig. 5; Supplementary Table 2). There are five ages of mainly igneous grains (Th/U>0.2) that fall within the uncertainty of the youngest peak at 364±3 Ma (MSWD=10).

The hornblende andesite (sample MM100320-4Ad) shows zircon U-Pb ages (concordia age and weighted mean $^{206}Pb/^{238}U$ ages) of 350±2 (n=9; MSWD=0.3; best age) and 356±2 Ma (n=11; MSWD=1.8) respectively (Fig. 4D; Supplementary Table 2). These ages are interpreted as the time of zoned igneous zircon crystallization and constrain the rock crystallization age.

The sandstone clast (sample MM060321-2Bd) in the pebbly shales shows a main peak at *ca.* 470 Ma and smaller peaks around *ca.* 340 Ma (younger peak at 340±2 Ma; n=3; MSWD=0.7; maximum depositional age), *ca.* 560 Ma and ca. 1000 Ma, besides two grains with Archean ages (Fig. 5; Supplementary Table 2).

The detrital zircons within the intrasparite (sample MM070322-03Dd) yield ages with peaks spanning from 342±2 Ma (n=4; MSWD=0.19; maximum depositional age) to *ca.* 1000 Ma. The most prominent age peak occurs at *ca.* 580 Ma, with a smaller peak at *ca.* 1400 Ma, and two Archaean grains (Fig. 5; Supplementary Table 2).

The paraconglomerate (sample MM160223-02d) yields a prominent peak at *ca.* 580 Ma, three ages within the uncertainty of the youngest peak at 345±2 Ma (MSWD=1.1), other peaks at *ca.* 740 Ma and ca. 1000 Ma, and four grains with Archean ages (Fig. 5; Supplementary Table 2).

In certain samples, a few individual zircon grains record anomalously young ages, best explained by localized Pb loss rather than a discrete geological event ($^{207}Pb/^{206}Pb$>0,06; see figures 3-5 and Supplementary Table 2).

5.4 Geochemistry

The Svea Granite is a peraluminous monzogranite (SiO_2=73 wt%; A/CNK>1; Supplementary Table 1) characterized by high K and Rb contents (Rb/Sr~2.3), pronounced enrichment in Large-Ion Lithophile Elements (LILE) relative to High Field Strength Elements (HFSE) (Rb/Hf~300; Rb/Zr~2.3), and strong depletion in chondrite-normalized Heavy Rare Earth Elements (HREE) (La/Yb_N~18.8; Dy/Yb~4.1; Gd/Yb~6.6) (Fig. 6). The granite also displays a pronounced negative Eu anomaly (Eu/Eu*=0.56), elevated Zr/Hf ratios (~127) and low to moderate Cr (10 ppm) and Ni (8 ppm) concentrations.

The hornblende andesite from the Paso Las Lagunas Formation (SiO_2=57 wt%; K_2O=0.8 wt%) exhibits chondrite-normalized LREE enrichment (La/Yb_N~9; Dy/Yb~2.1; Gd/Yb~2.6) (Fig. 6), no significant Eu anomaly (Eu/Eu*~1), and Sr (Sr/Y~29; Rb/Sr~0.04) and Zr (Zr/Hf~144) enrichment, together with low Cr (~7 ppm) and Ni (<5 ppm) concentrations.

6. Discussion

6.1 Petrogenesis of the Svea granite

This work reports the first finding of Devonian magmatic rocks in Tierra del Fuego within the Cordillera Darwin massif. From a geochemical perspective, the Svea

Granite is a peraluminous monzogranite with a transitional tectonic affinity between continental arc and collisional settings (Fig. 6A), displaying strong HREE depletion and a negative Eu anomaly (Fig. 6B, C). This suggests the involvement of refractory garnet-bearing residual assemblages in the magmatic source region (*e.g.,* Jung *et al.*, 2000) accompanied by fractionation of plagioclase and zircon during melt evolution (Fig. 6C, D). These features are consistent with the geochemical signature of silicic magmatism in subduction-related magmatic arcs and rift systems (*e.g.,* Rapela *et al.*, 2021, 2024) and post-collisional magmatic settings (*e.g.,* Guido *et al.*, 2005; Rojo *et al.*, 2021b). Consequently, we interpret these observations, together with the inherited zircon cores, as evidence of crustal anatexis within a continental arc to transitional (back-arc?) tectonic setting in the extensional foreland domain during the Middle to Late Devonian (*ca.* 393-377 Ma; Fig. 7).

6.2 Emplacement and exhumation of the Svea granite

The reported ages indicate that the Svea Granite crystallized at *ca.* 377 Ma and had cooled to shallow crustal levels by the Famennian, as recorded by a muscovite $^{40}Ar/^{39}Ar$ age of 363.4±1.3 Ma (Fig. 3B). Its exhumation is constrained to the Mississippian by a *ca.* 355 Ma U-Pb crystallization age obtained from an andesite within the upper section of the Paso Las Lagunas Formation. The host rock of the Svea Granite remains unknown, as it was not observed during fieldwork. Inherited zircon cores in the Svea Granite yield U-Pb ages from Precambrian (*ca.* 1074-595 Ma), Cambrian (*ca.* 516 Ma), Silurian (*ca.* 424 Ma), and Early Devonian (*ca.* 406 Ma) sources (Fig. 3C; Supplementary Table 2). Furthermore, the U-Pb zircon age of 387±3 Ma obtained from the orthogneiss cobble is interpreted as the crystallization age of a Middle Devonian plutonic protolith, consistent with the age reported for a gneiss from Target Hill in the Antarctic Peninsula (393±1 Ma; Millar *et al.*, 2002). Taken together, these data suggest that magmatism developed from the Middle to Late Devonian (Fig. 4C). These ages, together with the inherited zircon cores of the Svea Granite and detrital zircon populations of the Paso Las Lagunas Formation (Fig. 5; Supplementary Table 2), are consistent with reported ages for the TFIMC (Hervé *et al.*, 2010b; Fig. 5) and the Antarctic Peninsula basement (Millar *et al.*, 2002), suggesting that these complexes may have constituted part of the basement in the study area.

6.3 Devonian-Carboniferous glacial deposition and its regional implications

The lower section of the Paso Las Lagunas Formation is characterized by immature sandstones and arkosic sandstones with a weighted mean $^{206}Pb/^{238}U$ age of the main zircon population and a concordia age of *ca.* 376 Ma (Fig. 5), suggesting a calm and shallow subaqueous environment near the source area of the detritus: the Svea Granite (Fig. 2A, B). We could not determine whether the succession was deposited in a marine or lacustrine environment.

The upper section of the Paso Las Lagunas Formation comprises pebbly shales with load clasts (dropstones), rhythmic fine-grained wackestone, and sandstone-mudstone couplets (varves; Fig. 2C, F), all interpreted as glaciolacustrine or glaciomarine in origin. The additional occurrence of paraconglomerates with a silty-clayey matrix and sandstone interpreted as glaciofluvial in origin is collectively consistent with a glacial to periglacial depositional environment (*e.g.* Kennedy and Eyles, 2025). Similar lithological associations are reported in Paleozoic glacigenic deposits from South America (Isaacson *et al.*, 2008), Patagonia (Bahía La Lancha Formation; Riccardi, 1971; Poiré *et al.*, 1999), Antarctica (Pagoda Formation, Upper Crashsite Group and Whiteout Conglomerate unit; Matsch and Ojakangas, 1992; Curtis and Storey, 1996; Elliot *et al.*, 2015), and Karoo Basin (Dwyka till, Fitzroy till, Gale mud, and the Prince Albert Formation; Elliot *et al.*, 2016).

The maximum depositional age of the Paso Las Lagunas Formation postdates the cooling age of the Svea Granite (ca. 363 Ma), while the deposition of the underlying glacial succession must have begun before the crystallization of the intercalated andesite at *ca.* 350 Ma. Therefore, the Paso Las Lagunas Formation represents the first record of glacigenic rocks associated with the Devonian-Carboniferous boundary glaciation (Isaacson *et al.*, 2008; Lakin *et al.*, 2016; Rosa and Isbell, 2020) in Tierra del Fuego and Chilean Patagonia.

The top of the Paso Las Lagunas Formation, overlying the andesite, is marked by intrasparite, sandstone and paraconglomerates (Fig. 5) suggesting a warmer shallow transitional marine environment, possibly marking the termination of a glaciation (Isaacson *et al.*, 2008). These strata yielded young detrital zircon age peaks at 340±2 Ma (three-grain peak from sandstone clast in a pebbly shale), 342±2 Ma (four-grain peak from the intrasparite), and 345±2 Ma (three-grain peak from the paraconglomerate), indicating deposition that extended at least into the Middle Mississippian.

The Paso Las Lagunas Formation shows detrital zircon age patterns with significant Devonian, Cambrian and Precambrian (ca. 570-1000 Ma) peaks. The latter two are comparable with peaks in the Crashsite Group and FitzGerald Bluffs quartzites (Castillo *et al.*, 2017; Riley *et al.*, 2023), in the Whiteout Conglomerate unit (Castillo *et al.*, 2017), as in the TFIMC (Hervé *et al.*, 2010b) and the nEAMC (Hervé *et al.*, 2003, 2008; Augustsson *et al.*, 2006, 2016; Rojo *et al.*, 2021a) in southern Patagonia.

Only one sandstone clast within a paraconglomerate yielded a zircon age distribution dominated by the Famatinian magmatic arc (*ca.* 470 Ma; Rapela *et al*., 2018), a signature not observed in any other sample from the Paso Las Lagunas Formation. In southern Patagonia, relics of Ordovician igneous rocks have been reported exclusively as clasts in Permian sediments exposed in the Deseado Massif (Pankhurst *et al*., 2003) and at the base of the Tobífera Formation in the Cordillera Darwin (Hervé *et al*., 2010a); in the Antarctic Peninsula, clasts with Ordovician ages have been documented in the conglomerates of View Point (Riley *et al.,* 2023, and references therein). Collectively, these data indicate a detrital zircon provenance from Patagonia (Deseado Massif and Tierra del Fuego; Pankhurst *et al*., 2003; Hervé *et al.,* 2010b) and Antarctica (Target Hill and the Transantarctic Mountains; Burton-Johnson and Riley, 2015; Castillo *et al.,* 2017; Millar *et al.,* 2002; Riley *et al.,* 2023) for the Paso Las Lagunas Formation.

The southern extension of the Paso Las Lagunas Formation coincides with the Lapataia Formation in Argentina (Cao *et al.,* 2018, 2022). In addition, both units share similar lithologies, maximum depositional ages and detrital zircon sources (e.g., samples LAP01 and ENS108 from Cao *et al*., 2022; samples CD06 and CD12 from Torres Carbonell *et al*., 2026), suggesting a correlation between them. This challenges the previously proposed Middle Jurassic rift-related interpretation for the Lapataia Formation (Cao *et al*., 2022; Torres Carbonell *et al*., 2026) and supports a Late Devonian-early Carboniferous glacial and periglacial origin.

6.4 Geodynamic implications

Detrital zircon ages from the Paso Las Lagunas Formation (this study), the CDMC (Hervé *et al.*, 2010a), and the nEAMC in Chile (Hervé *et al.*, 2003, 2008; Augustsson *et al.*, 2006, 2016; Rojo *et al.*, 2021a), together with those from the Lapataia Formation in Argentina (Cao *et al.*, 2022; Torres Carbonell *et al.*, 2026), the View Point conglomerate unit in the Antarctic Peninsula (Bradshaw *et al.*, 2012), and Devonian paleogeographic reconstructions of southwest Gondwana (Lawver *et al.*, 2018; Riley *et al.*, 2023), indicate that Patagonia and the Antarctic Peninsula were in proximity during the Late Devonian to Mississippian. This raises the possibility that the Svea Granite is related to the Target Hill orthogneiss and associated granites, which exhibit similar mineralogy, crystallization age (*ca.* 395 Ma) and metamorphism age (*ca.* 327 Ma; Millar *et al.*, 2002); as well as to magmatism of the Deseado Massif, including the El Laurel Tonalite (*ca.* 395 Ma, Pankhurst *et al.*, 2003), the Laguna Larga Granite (*ca.* 362 Ma., Ballivián Justiniano *et al.*, 2023), and the Bahía Laura Granite (*ca.* 393 Ma, Guido *et al.*, 2005).

The geographical distribution of crystallization ages is consistent with a Devonian-Carboniferous magmatic arc developed across continental blocks now preserved in Patagonia and the Antarctic Peninsula (Pankhurst *et al.*, 2003, 2006; Ramos, 2008; Elliot *et al.*, 2015). These include the Deseado Massif (Pankhurst *et al.*, 2003; Ballivián Justiniano *et al.*, 2023; Guido *et al.*, 2005) and the nEAMC (Hervé *et al.*, 2003, 2007a; Pankhurst *et al.*, 2003; Augustsson *et al.*, 2006; Rojo *et al.*, 2021b) in southern Patagonia, the Target Hill Complex in the Antarctic Peninsula (Millar *et al.*, 2001, 2002; Riley *et al.*, 2023), and the Fosdick Mountains and Thurston Island in West Antarctica (Pankhurst *et al.*, 1998; Korhonen *et al.*, 2010; Elliot *et al.*, 2015; Riley *et al.*, 2017).

The Svea Granite and Paso Las Lagunas Formation show no evidence of Cretaceous metamorphism, preserving a distinct Paleozoic tectonothermal history. The crystallization and cooling of the Svea Granite at shallow crustal levels were followed by exhumation and erosion during the early Carboniferous, ultimately leading to the deposition of the Paso Las Lagunas Formation in a glacial to periglacial environment. This suggests a localized deformation and/or metamorphic event of uncertain nature in the region, accompanied by glacial denudation during the early Carboniferous. In this context, the presence of zircon rims with Permian U-Pb ages of *ca.* 272 Ma (Fig. 3A), some of which may represent metamorphic growth, suggests that the Paleozoic Svea Granite-Paso Las Lagunas Formation basement block may have been affected by a Permian thermal or tectonic event, potentially related to its position within or near a magmatic arc or rift zone, similar to the Permian tectonothermal history recorded in the TFIMC (Hervé *et al.*, 2010b; Castillo *et al.*, 2017).

In contrast, a back-arc basin floored by oceanic-type crust has been proposed for the nEAMC during the Late Devonian-early Carboniferous, with closure occurring in the early Carboniferous (Rojo *et al.*, 2021a, b). In the CDMC, however, there are no reported ultramafic or mafic rocks interpreted as remnants or protoliths of Paleozoic oceanic lithosphere (Nelson *et al.*, 1980; Cao *et al.*, 2018; Hervé *et al.*, 2010a). Within this geodynamic framework, the Svea Granite would have developed in an arc to transitional, potentially back-arc, setting, followed by uplift and andesitic magmatism in a continental-arc setting during the early Carboniferous (Fig. 7). The data presented here do not provide conclusive evidence that the sedimentation and magmatism in the study area occurred in a Late Devonian back-arc setting with oceanic crust development, as proposed to the north of the study area in the nEAMC (Rojo *et al.*, 2021b) where metabasalts and local serpentinite bodies with MORB-IAT-BABB affinities are exposed. If such a basin existed in the study area, it was likely shallow and may have deepened northward in a scissor-like configuration, with closure progressing from south to north during the early Carboniferous (Fig. 7).

Although the Svea Granite and Paso Las Lagunas Formation are presently exposed within the CDMC, their tectonothermal history differs markedly from that which experienced Cretaceous metamorphism associated with the Late Cretaceous closure of the Rocas Verdes Basin (Hervé *et al.*, 1981, 2010a; Dalziel and Brown, 1989; Kohn *et al.*, 1993; Cunningham, 1995; Suárez *et al.*, 2000; Klepeis *et al.*, 2010; Calderón *et al.*, 2012; Gallardo *et al.*, 2019, 2022; Torres Carbonell *et al.*, 2020; Muller *et al.* 2021), and subsequent collision of the drifted island arc. This collision may have also contributed to the development of metamorphism and mylonitization in the Cordillera Darwin region (Calderón *et al.*, 2021; Torres Carbonell and Cao, 2022; Cao *et al.*, 2023) (Fig. 7).

7. Conclusions

Field observations, petrographic studies and geochronological data presented in this study lead to the following conclusions:

1. The Svea Granite, with a crystallization age of *ca.* 375 Ma, represents the first documented occurrence of Late Devonian peraluminous magmatism in Tierra del Fuego and the Cordillera Darwin. Its age and regional distribution are consistent with a Devonian-Carboniferous magmatic arc developed across continental blocks now preserved in Patagonia and the Antarctic Peninsula. The granite subsequently underwent cooling and exhumation, as indicated by a $^{40}Ar/^{39}Ar$ muscovite age of *ca.* 363 Ma, followed by erosion and deposition of the Paso Las Lagunas Formation. The *ca.* 350 Ma age of an intercalated andesite indicates that exhumation

and erosion of the Svea Granite were broadly contemporaneous with deposition of the succession in a glacial to periglacial environment.

2. The sedimentary facies of the Paso Las Lagunas Formation support a glacial to periglacial depositional environment. The age of the lower part of the succession is constrained by the *ca.* 363 Ma $^{40}Ar/^{39}Ar$ muscovite age from the Svea Granite, whereas the overlying sedimentary units contain a youngest detrital zircon age peak of 340±2 Ma, indicating that deposition continued until at least this time. Together, these data constrain deposition of the Paso Las Lagunas Formation to the Late Devonian-Mississippian and indicate a minimum duration of 10 Myr. This represents the first documented evidence of Devonian–Mississippian glaciation in Tierra del Fuego.
3. These correlations suggest that the Paso Las Lagunas Formation may represent a Late Devonian–early Carboniferous glacial to periglacial succession rather than exclusively reflecting erosion of a Paleozoic basement during the Middle Jurassic rifting of the Rocas Verdes Basin.

8. Acknowledgements

The authors gratefully acknowledge the professionals of Sernageomin who participated in the sample processing for mineral separation and preparation of rock thin sections. Special thanks are given to M. Suárez, from the Geochronology Laboratory of Sernageomin, and V. Valencia from ZirChron LLC (Arizona, USA), for their rigor in the geochronological analyses performed. We thank E. Rogel, R. Santibáñez, and D. Cárdenas for their logistical support in fieldwork. We also gratefully acknowledge M. Sánchez for his valuable assistance with the petrographic descriptions. Additionally, we thank colleagues F. Hervé (Andrés Bello University; Proyecto Exploración 13220141), P. Mella and D. González (ENAP), L. Rojas (Sipretrol), and A. Díaz (Sernageomin) for their support, provision of bibliography, manuscript correction, fieldwork, and fruitful discussions. Finally, we thank P. Quezada, C. Ramírez de Arellano and M. Calderón for their careful review of the manuscript and valuable contributions to its final version.

9. References

Augustsson, C.; Münken, C.; Bahlburg, H.; Fanning, M. 2006. Provenance of late Palaeozoic metasediments of the SW South American Gondwana margin: a combined U–Pb and Hf-isotope study of single detrital zircons. Journal of the Geological Society 163 (6): 983–995.

Augustsson, C.; Willner, A.P.; Rüsing, T.; Niemeyer, H.; Gerdes, A.; Adams, C.J.; Miller, H. 2016. The crustal evolution of South America from a zircon Hf-isotope perspective. Terra Nova 28 (2): 128–137.

Bahlburg, H. 2022. A Silurian-Devonian active margin in the proto-Andes – new data on an old conundrum. International Geology Review 64 (21): 3099–3120.

Ballivián Justiniano, C.A.; Oriolo, S.; Basei, M.A.S. 2023a. Coupled U–Pb and Lu–Hf zircon data of Late Devonian magmatism from Bajo de La Leona (Deseado Massif, Argentina): Tracking the southernmost exposure of the Devonian magmatic arc of Patagonia. Journal of South American Earth Sciences 128: 104455.

Barbeau, D.L.; Olivero, E.B.; Swanson-Hysell, N.L.; Zahid, K.M.; Murray, K.E.; Gehrels, G.E. 2009. Detrital-zircon geochronology of the eastern Magallanes foreland basin: Implications for Eocene kinematics of the northern Scotia Arc and Drake Passage. Earth and Planetary Science Letters 284 (3–4): 489–503.

Betka, P., Mosher, S. Klepeis, K. 2022. Progressive Development of a Distributed Ductile Shear Zone beneath the Patagonian Retroarc Fold-Thrust Belt, Chile. Lithosphere, 1, 3820115.

Bradshaw, J.; Vaughan, A.; Millar, I.; Flowerdew, M.J.; Trouw, R.; Fanning, M.; Whitehouse, M.J. 2012. Permo-Carboniferous conglomerates in the Trinity Peninsula Group at View Point, Antarctic Peninsula: sedimentology, geochronology and isotope evidence for provenance and tectonic setting in Gondwana. Geological Magazine 149 (4): 626–644.

Burton-Johnson, A.; Riley, T.R. 2015. Autochthonous v. accreted terrane development of continental margins: a revised in situ tectonic history of the Antarctic Peninsula. Journal of the Geological Society 172 (6): 822–835.

Calderón, M.; Fosdick, J.C.; Warren, C.; Massonne, H.-J.J.; Fanning, C.M.; Cury, L.F.; Schwanethal, J.; Fonseca, P.E.; Galaz, G.; Gaytán, D.; Hervé, F. 2012. The low-grade Canal de las Montañas Shear Zone and its role in the tectonic emplacement of the Sarmiento Ophiolitic Complex and Late Cretaceous Patagonian Andes orogeny, Chile. Tectonophysics 524–525: 165–185.

Calderón, M.; Hervé, F.; Fuentes, F.; Fosdick, J.; Sepúlveda, F.; Galaz, G. 2016. Tectonic Evolution of Paleozoic and Mesozoic Andean Metamorphic Complexes and the Rocas Verdes Ophiolites in Southern Patagonia. *In* Geodynamic Evolution of the Southernmost Andes (Ghiglione, M.; editor). Springer Earth System Sciences: 7–37. Switzerland.

Calderón, M.; Zuñiga, C.; Hervé, F.; Theye, T.; Galaz, G.; Rojo, D.; Suárez, R. 2021. Barrovian-type metamorphism in the western domain of the Cordillera Darwin Metamorphic Complex, Fuegian Andes. *In* EGU General Assembly: EGU: Alemania.

Cao, S. J.; Blanc, P.A.; Dimieri, L. 2018. Structural and petrographic constraints on the stratigraphy of the Lapataia Formation, with implications for the tectonic evolution of the Fuegian Andes. Journal of South American Earth Sciences 84: 223–241.

Cao, S. J.; Torres Carbonell, P.J.; Bordese, S.; Lovecchio, J. 2022. Early rifting during marginal basin development: Petrography, microstructure, and detrital zircon U-Pb geochronology of the Lapataia Formation, Argentine Fuegian Andes. Basin Research 34 (00): 1–21.

Cao, S. J.; Torres Carbonell, P.J.; Sánchez, N.P.; Bordese, S.; Dimieri, L.V. 2023. Thrust tectonics in the Fuegian Andes central belt: A detailed geometric-kinematic analysis and new thermochronological constraints. Tectonophysics 862: 229966.

Castillo, P.; Fanning, C.M.; Fernandez, R.; Poblete, F.; Hervé, F. 2017. Provenance and age constraints of Paleozoic siliciclastic rocks from the Ellsworth Mountains in West Antarctica, as determined by detrital zircon geochronology. GSA Bulletin 129 (11–12): 1568–1584.

Castillo, P., Fanning, C.M., Hervé, F., Lacassie, J.P. 2016. Characterisation and tracing of Permian magmatism in the south-western segment of the Gondwanan margin; U–Pb age, Lu–Hf and O isotopic compositions of detrital zircons from metasedimentary complexes of northern Antarctic Peninsula and western Patagonia. Gondwana Research, 10.1016/j.gr.2015.07.014.

Cawood, P.A. 2005. Terra Australis Orogen: Rodinia breakup and development of the Pacific and Iapetus margins of Gondwana during the Neoproterozoic and Paleozoic. Earth-Science Reviews 69 (3–4): 249–279.

Cerredo, M.E.; Tassone, A.; Rapalini, A.; Hervé, F.; Fanning, M. 2011. Campanian magmatism in the Fuegian Andes: new SHRIMP age of Jeujepén pluton. *In* XVIII Congreso Geológico Argentino. S12 Tectónica Andina: 2. Neuquén.

Cunningham, W.D. 1995. Orogenesis at the southern tip of the Americas: the structural evolution of the Cordillera Darwin metamorphic complex, southernmost Chile. Tectonophysics 244 (4): 197–229.

Curtis, M.L.; Storey, B. 1996. A review of geological constraints on the pre-break-up position of the Ellsworth Mountains within Gondwana: implications for Weddell Sea evolution. Geological Society, London, Special Publications 108 (1): 11–30.

Dalziel, I.W.D.; Brown, R.L. 1989. Tectonic denudation of the Darwin metamorphic core complex in the Andes of Tierra del Fuego, southernmost Chile: Implications for Cordilleran orogenesis. Geology 17 (8): 699–703.

Darwin, C. 1846. Geological observations on South America. Smith, Elder and Co., 65, Cornhill.: 279 p. London.

Elliot, D.H. 2013. The geological and tectonic evolution of the Transantarctic Mountains: a review. Geological Society, London, Special Publications 381 (1): 7–35.

Elliot, D.H.; Fanning, C.M.; Hulett, S.R.W. 2015. Age provinces in the Antarctic craton: Evidence from detrital zircons in Permian strata from the Beardmore Glacier region, Antarctica. Gondwana Research 28 (1): 152–164.

Elliot, D.H.; Fanning, C.M.; Laudon, T.S. 2016. The Gondwana Plate margin in the Weddell Sea sector: Zircon geochronology of Upper Paleozoic (mainly

Permian) strata from the Ellsworth Mountains and eastern Ellsworth Land, Antarctica. Gondwana Research 29 (1): 234–247.
Gallardo, R.; Ghiglione, M.C.; Rojas, L. 2019. Tectonic evolution of the Southern Austral-Magallanes Basin in Tierra Del Fuego. Latin American Journal of Sedimentology and Basin Analysis 26 (2 SE-): 127–154.
Gallardo, R.; Ghiglione, M.C.; Rojas, L.; Mpodozis, C. 2022. From rift to foreland basin: A case example from the Austral basin, southernmost Andes. Basin Research 35 (3): 865–897.
González-Guillot, M.; Ghiglione, M.C.; Escayola, M.; Martins Pimentel, M.; Mortensen, J.; Acevedo, R. 2018. Ushuaia pluton: Magma diversification, emplacement and relation with regional tectonics in the southernmost Andes. Journal of South American Earth Sciences 88: 497–519.
Guido, D.; Rapela, C.; Pankhurst, R.; Fanning, C. 2005. Edad del granito del afloramiento Bahía Laura, Macizo del Deseado, provincia de Santa Cruz. *In* 16° Congreso Geológico Argentino, No. 1: 85–88. La Plata.
Heredia, N.; García-Sansegundo, J.; Gallastegui, G.; Farias, P.; Giacosa, R.E.; Hongn, F.; Tubía, J.M.; Alonso, J.L.; Busquets, P.; Charrier, R.; Clariana, P.; Colombo, F.; Cuesta, A.; Gallastegui, J.; Giambiagi, L.; González-Menéndez, L.; Limarino, C.O.; Martín-González, F.; Pedreira, D.; Quintana, L.; Rodríguez Fernández, L.R.; Rubio-Ordóñez, A.; Seggiaro, R.; Serra-Varela, S.; Spalletti, L.A.; Cardó, R.; Ramos, V.A. 2018. The Pre-Andean Phases of Construction of the Southern Andes Basement in Neoproterozoic–Paleozoic Times. *In* The evolution of the Chilean-Argentinean Andes (Folguera, A.; Contreras-Reyes, E.; Heredia, N.; Encinas, A.; Iannelli, S.B.; Oliveros, V.; Dávila, F.M.; Collo, G.; Giambiagi, L.; Maksymowicz, A.; Iglesia Llanos, M.P.; Turienzo, M.; Naipauer, M.; Orts, D.; Litvak, V.D.; Álvarez, O.; Arriagada, C.; editors). Springer-Verlag: 111–131. Cham.
Hervé, F.; Calderón, M.; Fanning, C.M.; Kraus, S.; Pankhurst, R.J.; Fanning, C.M.; Kraus, S.; Pankhurst, R.J. 2010b. SHRIMP chronology of the Magallanes Basin basement, Tierra del Fuego: Cambrian plutonism and Permian high-grade metamorphism. Andean Geology 37 (2): 253–275.
Hervé, F.; Calderon, M.; Fanning, C.M.; Pankhurst, R.J.; Fuentes, F.; Rapela, C.W.; Correa, J.; Quezada, P.; Marambio, C. 2016. Devonian magmatism in the accretionary complex of Southern Chile. Journal of the Geological Society 173 (4): 587–602.
Hervé, F.; Calderón, M.; Faúndez, V. 2008. The metamorphic complexes of the Patagonian and Fuegian Andes. Geologica Acta 6 (1): 43–53.
Hervé, F.; Fanning, C.M.; Pankhurst, R.J. 2003. Detrital zircon age patterns and provenance of the metamorphic complexes of southern Chile. Journal of South American Earth Sciences 16 (1): 107–123.
Hervé, F.; Fanning, C.M.; Pankhurst, R.J.; Mpodozis, C.; Klepeis, K.; Calderón, M.; Thomson, S.N. 2010a. Detrital zircon SHRIMP U-Pb age study of the Cordillera Darwin Metamorphic Complex of Tierra del Fuego: Sedimentary sources and implications for the evolution of the Pacific margin of Gondwana. Journal of the Geological Society 167 (3): 555–568.
Hervé, F.; Faundez, V.; Calderón, M.; Massonne, H.-J.; Willner, A. 2007a. Metamorphic and plutonic basement complexes. *In* The Geology of Chile

(Moreno, T.; Gibbons, W.; editors). Geological Society Special Publication: 5–19. London.
Hervé, F.; Nelson, E.; Kawashita, K.; Suárez, M. 1981. New isotopic ages and the timing of orogenic events in the Cordillera Darwin, southernmost Chilean Andes. Earth and Planetary Science Letters 55 (2): 257–265.
Hervé, F.; Nelson, E.; Suarez, M. 1979. Edades Radiométricas de Granitoides y Metamofitas Provenientes de Cordillera Darwin, XII Región, Chile. Revista Geológica de Chile 7: 31–40.
Hervé, F.; Pankhurst, R.J.; Fanning, C.M.; Calderón, M.; Yaxley, G.M. 2007b. The South Patagonian batholith: 150 my of granite magmatism on a plate margin. Lithos 97 (3–4): 373–394.
Isaacson, P.E.; Díaz-Martínez, E.; Grader, G.W.; Kalvoda, J.; Babek, O.; Devuyst, F.X. 2008. Late Devonian–earliest Mississippian glaciation in Gondwanaland and its biogeographic consequences. Palaeogeography, Palaeoclimatology, Palaeoecology 268 (3): 126–142.
Jung, S.; Hoernes, S.; Mezger, K. 2000. Geochronology and petrology of migmatites from the Proterozoic Damara Belt — importance of episodic fluid-present disequilibrium melting and consequences for granite petrology. Lithos 51 (3): 153–179.
Kennedy, K.; Eyles, N. 2025. The Paleoproterozoic (c. 2.3 Ga) Gowganda Formation: Deep water, glacially-influenced debrites and related mass flow along a passive margin. Earth-Science Reviews 261: 105033.
Klepeis, K.; Betka, P.; Clarke, G.; Fanning, M.; Hervé, F.; Rojas, L.; Mpodozis, C.; Thomson, S. 2010. Continental underthrusting and obduction during the Cretaceous closure of the Rocas Verdes rift basin, Cordillera Darwin, Patagonian Andes. Tectonics 29 (3): 2009TC002610.
Kohn, M.J.; Spear, F.S.; Dalziel, I.W.D. 1993. Metamorphic P-T Paths from Cordillera Darwin, a Core Complex in Tierra del Fuego, Chile. Journal of Petrology 34 (3): 519–542.
Kohn, M.J.; Spear, F.S.; Harrison, T.M.; Dalziel, W.D. 1995. 40Ar/39Ar geochronology and P-T-t paths from the Cordillera Darwin metamorphic complex, Tierra del Fuego, Chile. Journal of Metamorphic Geology 13: 251–270.
Korhonen, F.J.; Saito, S.; Brown, M.; Siddoway, C.S.; Day, J.M.D. 2010. Multiple Generations of Granite in the Fosdick Mountains, Marie Byrd Land, West Antarctica: Implications for Polyphase Intracrustal Differentiation in a Continental Margin Setting. Journal of Petrology 51 (3): 627–670.
Lanphere, M.A.; Baadsgaard, H. 2001. Precise K–Ar, 40Ar/39Ar, Rb–Sr and U/Pb mineral ages from the 27.5 Ma Fish Canyon Tuff reference standard. Chemical Geology 175 (3): 653–671.
Lakin, J.A.; Marshall, J.E.; Trot, I.; Harding, I.C. 2016. Greenhouse to icehouse: a biostratigraphic review of latest Devonian–Mississippian glaciations and their global effects. Geological Society, London, Special Publications 423 (1): 439–464.
Lawver, L.A.; Dalziel, I.W.D.; Norton, I.O.; Gahagan, L.M.; Davis, J. 2018. The PLATES 2014 Atlas of Plate Reconstructions (550 Ma to Present Day), PLATES Progress Report No. 374-0215: 220p.

Ludwig, K.R. 2012. Isoplot v. 3.75: A Geochronological Toolkit for Microsoft Excel. Berkeley Geochronology Center, Berkeley Geochronology Center Special Publication, Special Publication 4: 75 p. California.

Malkowski, M.A.; Grove, M.; Graham, S.A. 2016. Unzipping the Patagonian Andes-Long-lived influence of rifting history on foreland basin evolution. Lithosphere 8 (1): 23–28.

Maloney, K.T.; Clarke, G.L.; Klepeis, K.A.; Fanning, C.M.; Wang, W. 2011. Crustal growth during back-arc closure: Cretaceous exhumation history of cordillera darwin, southern patagonia. Journal of Metamorphic Geology 29 (6): 649–672.

Matsch, C.L.; Ojakangas, R.W. 1992. Stratigraphy and sedimentology of the Whiteout Conglomerate; An upper Paleozoic glacigenic unit, Ellsworth Mountains, West Antarctica. In Geology and Paleontology of the Ellsworth Mountains, West Antarctica (Webers, G.F.; Craddock, C.; Splettstoesser, J.F.; editors). Geological Society of America: 37–62.

Mella, M.; Quiroz, D.; Díaz, A.; Opazo, E. 2025. Geología básica y aplicada del área Bahía Blanca-Caleta Benavente, región de Magallanes y de la Antártica Chilena. Servicio Nacional de Geología y Minería: 167 p. Santiago, Chile.

Merdith, A.S.; Williams, S.E.; Collins, A.S.; Tetley, M.G.; Mulder, J.A.; Blades, M.L.; Young, A.; Armistead, S.E.; Cannon, J.; Zahirovic, S.; Müller, R.D. 2021. Extending full-plate tectonic models into deep time: Linking the Neoproterozoic and the Phanerozoic. Earth-Science Reviews 214: 103477.

Millar, I.L.; Pankhurst, R.J.J.; Fanning, C.M. 2002. Basement chronology of the Antarctic Peninsula: recurrent magmatism and anatexis in the Palaeozoic Gondwana Margin. Journal of the Geological Society 159 (2): 145–157.

Millar, I.L.; Willan, R.C.R.R.; Wareham, C.D.; Boyle, A.J.; Boyce, A.J. 2001. The role of crustal and mantle sources in the genesis of granitoids of the Antarctic Peninsula and adjacent crustal blocks. Journal of the Geological Society 158 (5): 855–867.

Milne, A.J.; Millar, I.L. 1989. Short paper: The significance of mid-Palaeozoic basement in Graham Land, Antarctic Peninsula. Journal of the Geological Society 146 (2): 207–210.

Mukasa, S.B.; Dalziel, I.W.D. 1996. Southernmost Andes and South Georgia Island, North Scotia Ridge: Zircon U-Pb and muscovite 40Ar/39Ar age constraints on tectonic evolution of Southwestern Gondwanaland. Journal of South American Earth Sciences 9 (5–6): 349–365.

Muller, V.; Calderón, M.; Fosdick, J.C.; Ghiglione, M.C.; Cury, L.F.; Massonne, H.-J.; Fanning, C.M.; Warren, C.J.; Ramírez de Arellano, C.; Sternai, P. (2021) The closure of the Rocas Verdes Basin and early tectono- metamorphic evolution of the Magallanes Fold-and-Thrust Belt, southern Patagonian Andes (52-54°S). Tectonophysics, 798, 228686.

Nelson, E.P. 1982. Post-tectonic uplift of the Cordillera Darwin orogenic core complex: evidence from fission track geochronology and closing temperature -time relationships. Journal of the Geological Society 139 (6): 755–761.

Nelson, E.P.; Dalziel, I.W.D.; Milnes, G. 1980. Structural geology of the Cordillera Darwin-collisional-style orogenesis in the southernmost Chilean Andes. *In* Eclogae Geologicae Helvetiae, No. 73, 3: 727–751.

Pankhurst, R.J. 1990. The Paleozoic and Andean magmatic arcs of West Antarctica and southern South America.
Pankhurst, R.J.; Rapela, C.W.; Fanning, C.M.; Márquez, M. 2006. Gondwanide continental collision and the origin of Patagonia. Earth-Science Reviews 76 (3–4): 235–257.
Pankhurst, R.J.; Rapela, C.W.; Loske, W.P.; Márquez, M.; Fanning, C.M. 2003. Chronological study of the pre-Permian basement rocks of southern Patagonia. Journal of South American Earth Sciences 16 (1): 27–44.
Pankhurst, R.; Weaver, S.; Bradshaw, J.; Storey, B.; Ireland, T. 1998. Geochronology and geochemistry of pre-Jurassic superterranes in Marie Byrd Land, Antarctica. Journal of Geophysical Research 103: 2529–2547.
Pearce, J.A.; Harris, N.B.W.; Tindle, A.G. 1984. Trace element discrimination diagrams for the tectonic interpretation of granitic rocks. Journal of Petrology 25 (4): 956–983.
Permuy Vidal, C.; Moreira, P.; Guido, D.M.; Fanning, C.M. 2014. Linkages between the southern Patagonia Pre-Permian basements: new insights from detrital zircons U-Pb SHRIMP ages from the Cerro Negro District. Geologica Acta: an international earth science journal 12 (2): 137–150.
Poiré, D.; Morel, E.; Maggi, J. 1999. Facies diamictíticas en la Formación Bahía de la Lancha (Paleozoico), Estancia La Lila, Lago San Martín, provincia de Santa Cruz, Argentina. *In* XIV Congreso Geológico Argentino. Actas I: 425–428. Salta, Argentina.
Quensel, P.D. 1910. Geologisch-petrographische Studien in der patagonischen Cordillera. Bulletin of the Geological Institution of the University of Upsala 11: 1–114.
Rapela, C.; García, M.; Hervé, F.; Pankhurst, R.; Calderón, M.; Fanning, C.; Verdecchia, S. 2024. Late Paleozoic magmatism and foreland deformation associated with opening and closing of marginal basins in the North Patagonian Andes. Journal of the Geological Society 181 (2): jgs2023-171.
Rapela, C.W.; Hervé, F.; Pankhurst, R.J.; Calderón, M.; Fanning, C.M.; Quezada, P.; Poblete, F.; Palape, C.; Reyes, T. 2021. The Devonian accretionary orogen of the North Patagonian cordillera. Gondwana Research 96: 1–21.
Riccardi, A. 1971. Estratigrafía en el oriente de la Bahía de la Lancha, Lago San Martín, Santa Cruz, Argentina. Revista del Museo de La Plata 7: 215–318.
Riley, T.R.; Burton-Johnson, A.; Flowerdew, M.J.; Poblete, F.; Castillo, P.; Hervé, F.; Leat, P.T.; Millar, I.L.; Bastias, J.; Whitehouse, M.J. 2023. Palaeozoic – Early Mesozoic geological history of the Antarctic Peninsula and correlations with Patagonia: Kinematic reconstructions of the proto-Pacific margin of Gondwana. Earth-Science Reviews 236: 104265.
Riley, T.R.; Flowerdew, M.J.; Pankhurst, R.J.; Leat, P.T.; Millar, I.L.; Fanning, C.M.; Whitehouse, M.J. 2017. A revised geochronology of Thurston Island, West Antarctica, and correlations along the proto-Pacific margin of Gondwana. Antarctic Science 29 (1): 47–60.
Rojo, D.; Calderón, M.; Ghiglione, M.C.; Suárez, R.J.; Quezada, P.; Cataldo, J.; Hervé, F.; Charrier, R.; Galaz, G.; Suárez, M.; Guettner, G.; Babinski, M. 2021a. The low-grade basement at Península La Carmela, Chilean Patagonia: new data for unraveling the pre-Permian basin nature of the Eastern Andean

Metamorphic Complex. International Journal of Earth Sciences 110 (6): 2021–2042.
Rojo, D.; Calderón, M.; Hervé, F.; Díaz, J.; Quezada, P.; Suárez, R.; Ghiglione, M.C.; Fuentes, F.; Theye, T.; Cataldo, J.; Sándoval, J.; Viefhaus, T. 2021b. Petrology and tectonic evolution of late Paleozoic mafic-ultramafic sequences and the Leones Pluton of the Eastern Andean Metamorphic Complex (46-47°S), southern Chile. Journal of South American Earth Sciences 108: 103198.
Rosa, E.L.M.; Isbell, J.L. 2020. Late Paleozoic Glaciation. *In* Reference Module in Earth Systems and Environmental Sciences. 534–545.
Sepúlveda, F.A.; Hervé, F.; Calderón, M.; Lacassie, J.P. 2008. Petrological and geochemical characteristics of metamorphic and igneous units from the allochthonous Madre de Dios Terrane, Southern Chile. Gondwana Research 13 (2): 238–249.
Söllner, F.; Miller, H.; Hervé, M. 2000. An Early Cambrian granodiorite age from the pre-Andean basement of Tierra del Fuego (Chile): the missing link between South America and Antarctica? Journal of South American Earth Sciences 13 (3): 163–177.
Suárez, M.; De La Cruz, R.; Bell, C.M. 2000. Timing and origin of deformation along the Patagonian fold and thrust belt. Geological Magazine 137 (4): 345–353.
Sun, S.S.; McDonough, W.F. 1989. Chemical and isotopic systematics of oceanic basalts: Implications for mantle composition and processes. Geological Society Special Publication 42 (1): 313–345.
Torres Carbonell, P.J.; Cao, S. 2022. Cuantificación de la deformación por cizalla simple vs. cizalla pura en milonitas de los Andes Fueguinos. *In* Congreso Geológico Argentino, No. 21, Sesión Temática 2: 141–142. Puerto Madryn, Argentina.
Torres Carbonell, P.J.; Cao, S.J.; González- Guillot, M.; Mosqueira González, V.; Dimieri, L.V.; Duval, F.; Scaillet, S. 2020. The Fuegian thrust-fold belt: From arc-continent collision to thrust-related deformation in the southernmost Andes. Journal of South American Earth Sciences 102: 102678.
Torres Carbonell, P.J.; Cao, S.J.; Poblete, F.A.; Poujol, M. 2026. Stratigraphic and structural reappraisal of the metamorphic complex of NE Cordillera Darwin, Tierra del Fuego, Chile. Andean geology 53: 176–205.
Vaughan, A.P.M.; Pankhurst, R.J. 2008. Tectonic overview of the West Gondwana margin. Gondwana Research 13 (2): 150–162.
Velásquez, R.; Bastias, J.; Salazar, E.; Poblete, F.; Guillot, M.G.; Chew, D.; Peña, M.; Tapia, F.; Ramirez, A.; Drakou, F. 2023. Magmatic arc evolution during the tectonic closure of the Rocas Verdes basin: insights from Cretaceous–earliest Paleocene intrusive rocks of Navarino Island (55°S), Fuegian Andes. Journal of the Geological Society 180 (5): jgs2022-163.
Vermeesch, P. 2018. IsoplotR: A free and open toolbox for geochronology. Geoscience Frontiers 9 (5): 1479–1493.

Figure Captions

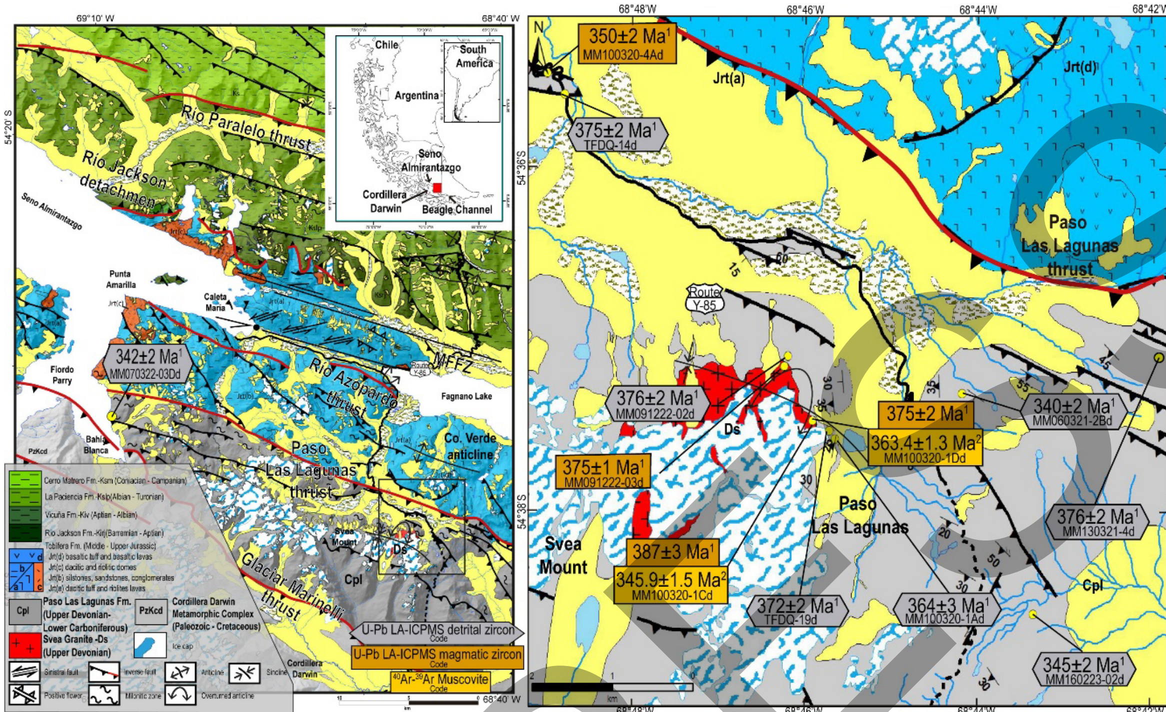

Fig. 1. Geology of the northeastern flank of Cordillera Darwin (modified from Mella *et al.*, 2025). The section highlights sample locations and the ages obtained in this study. Numbers in superscripts are (1) weighted average younger detrital zircon age or weighted average of magmatic zircon and (2) $^{40}Ar/^{39}Ar$ plateau age. MFFZ: Magallanes-Fagnano Fault Zone. See Table 1 for sample locations.

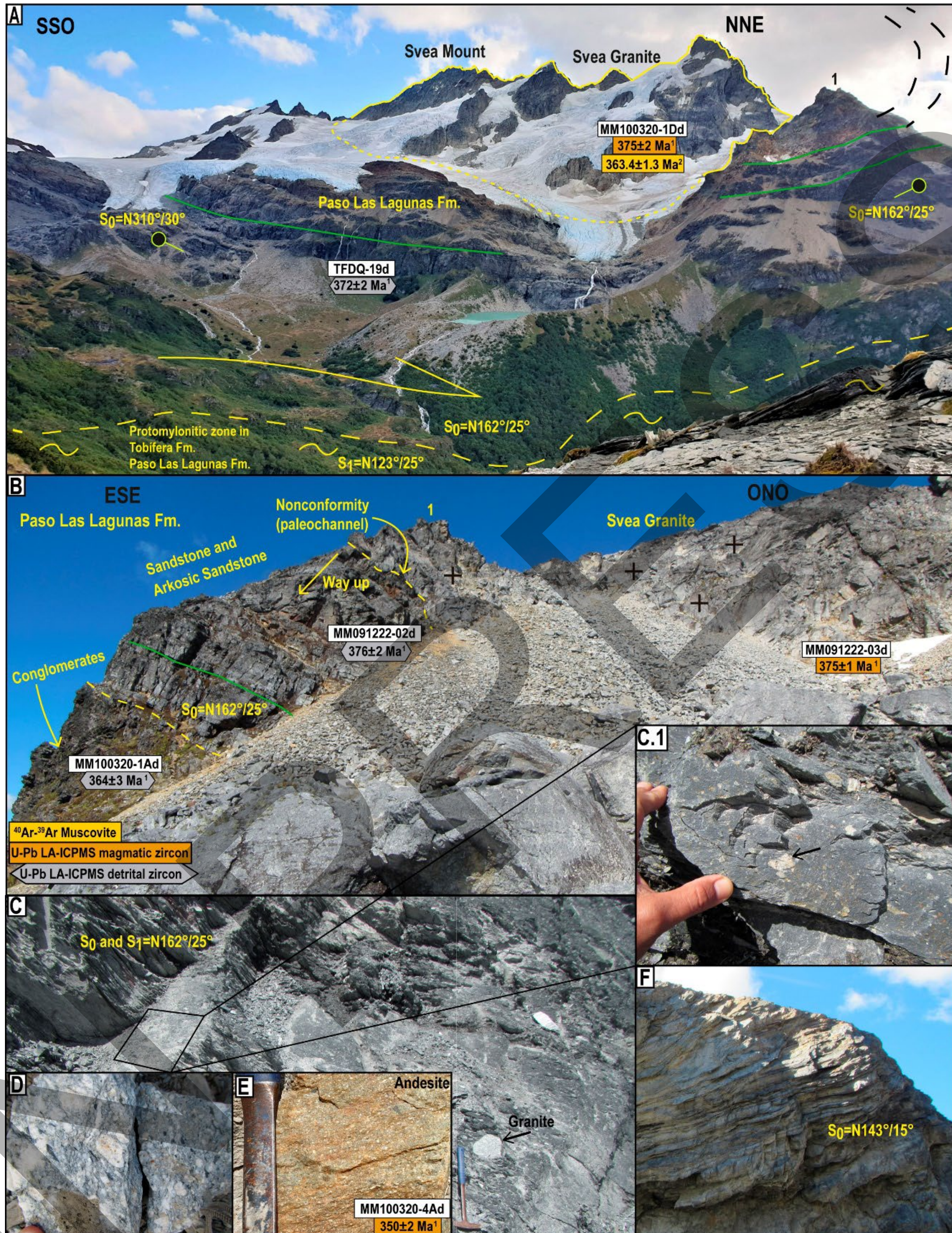

Fig. 2. A. Svea mount standing out in the core of the overturned anticline composed of Svea Granite and the Paso Las Lagunas Formation, with a lower mylonite interpreted as a detachment zone (view to the west). The synform is currently being configured. **B.** Nonconformity between the Paso Las Lagunas Formation and the

Svea Granite (view to the east), highlighting the ages and inverted polarity. **C.** Pebbly shale with dispersed granite lithics (the arrow indicates a faceted block). **C.1.** Detailed view of pebbles embedded in a mud matrix. **D.** Conglomerate rich in granite lithics, arkoses and mudstones. **E.** Andesite of *ca.* 355 Ma. **F.** Rhythmic succession of mudstones interpreted as varves. Numbers in superscripts in panels A, B and D are (1) weighted average younger detrital zircon age or weighted average of magmatic zircon and (2) $^{40}Ar/^{39}Ar$ plateau age. See Table 1 for sample locations.

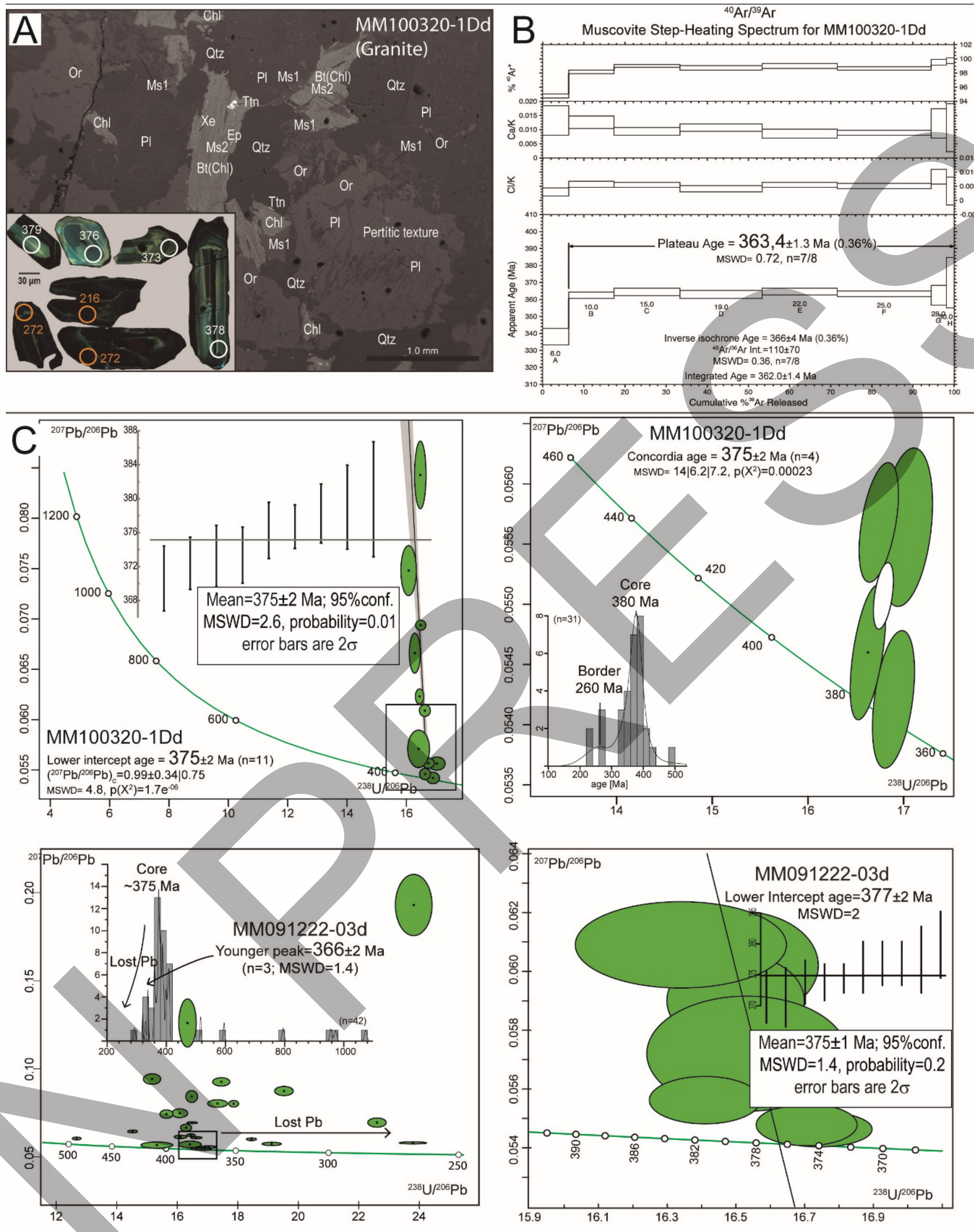

Fig. 3. Svea Granite, monzogranite. **A.** Zircon cathodoluminescence (CL) and backscattered electron (BSE) images. **B.** Plateau $^{40}Ar/^{39}Ar$ diagram. **C.** Tera-Wasserburg diagrams showing ages vs probabilities, concordia ages, and weighted mean $^{206}Pb/^{238}U$ ages for igneous crystallization. Lost Pb shown for sample

MM091222-03d. MSWD: Mean Squared Weighted Deviation. Bt: biotite; Chl: chlorite; Ep: epidote; Ms: muscovite; Or: orthoclase; Pl: plagioclase; Qtz: quartz; Ttn: titanite; Xe: xenotime.

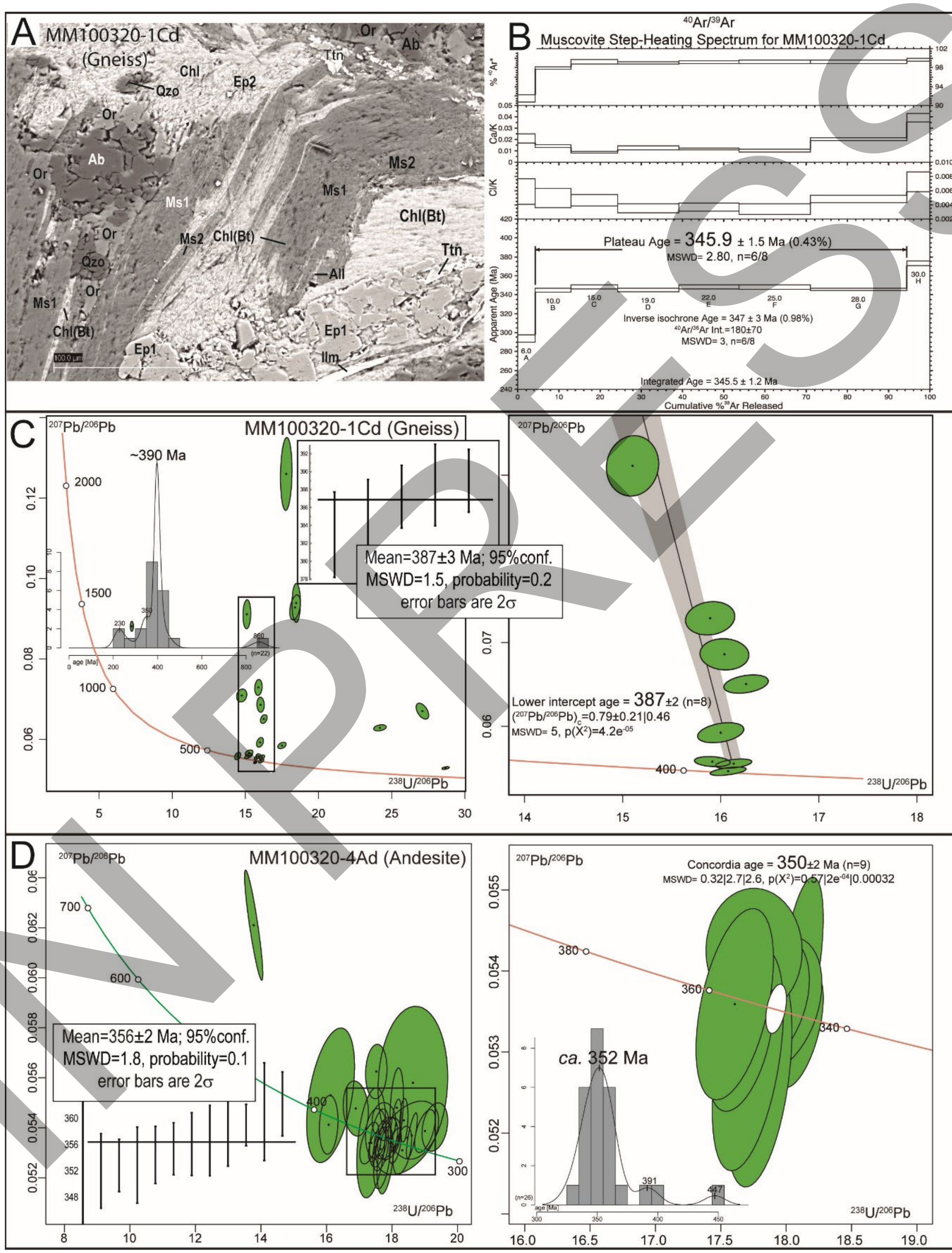

Fig. 4. Svea Granite, orthogneiss. **A.** Backscattered electron (BSE) image. **B.** Plateau $^{40}Ar/^{39}Ar$ diagram. **C.** Tera-Wasserburg diagrams, showing ages vs probabilities, concordia ages and weighted mean $^{206}Pb/^{238}U$ ages diagrams for orthogneiss igneous crystallization. **D.** Paso Las Lagunas Formation, andesite age data. Tera-Wasserburg diagrams, showing concordia ages and weighted mean $^{206}Pb/^{238}U$ ages for andesite igneous crystallization. MSWD: Mean Squared Weighted Deviation. Ab: albite; Bt: biotite; Chl: chlorite; Ep: epidote; Ilm: Ilmenite; Ms: muscovite; Or: orthoclase; Qtz: quartz; Ttn: titanite.

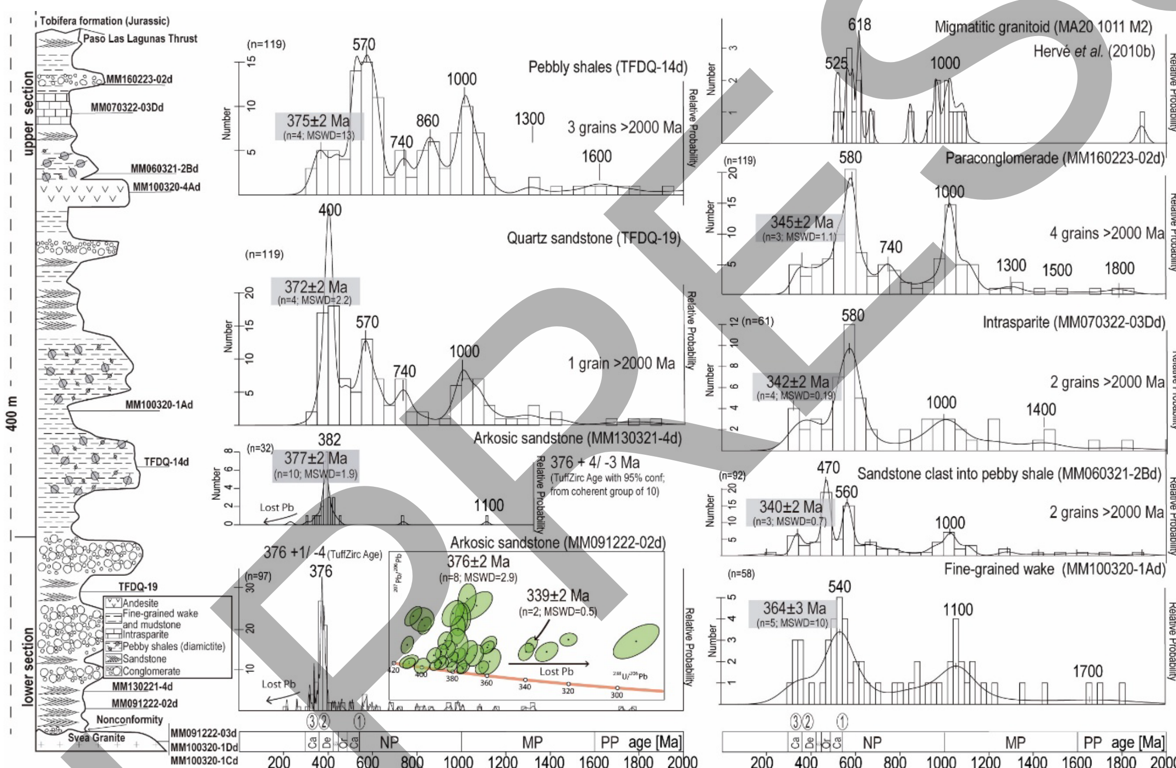

Fig. 5. Paso Las Lagunas Formation. Generalized stratigraphic column and multiple age histograms and probability plots for dated samples. A Tera-Wasserburg diagram was incorporated to the arkosic sandstone MM091222-02d, in which the data define an array parallel to the x-axis at nearly constant $^{207}Pb/^{206}Pb$, interpreted as recent Pb loss. For comparison with the TFIMC, a migmatitic granitoid is shown (Hervé et al., 2010b). 1. Tierra del Fuego Igneous and Metamorphic Complex (TFIMC) and Ross Orogen; 2. Svea Granite magmatic zircon population; 3. Andesite of the Paso Las Lagunas Formation. NP: Neoproterozoic; MP: Mesoproterozoic; PP:

Paleoproterozoic. Ca: Carboniferous; De: Devonian; Si: Silurian; Or: Ordovician; Ca: Cambrian. MSWD: Mean Squared Weighted Deviation.

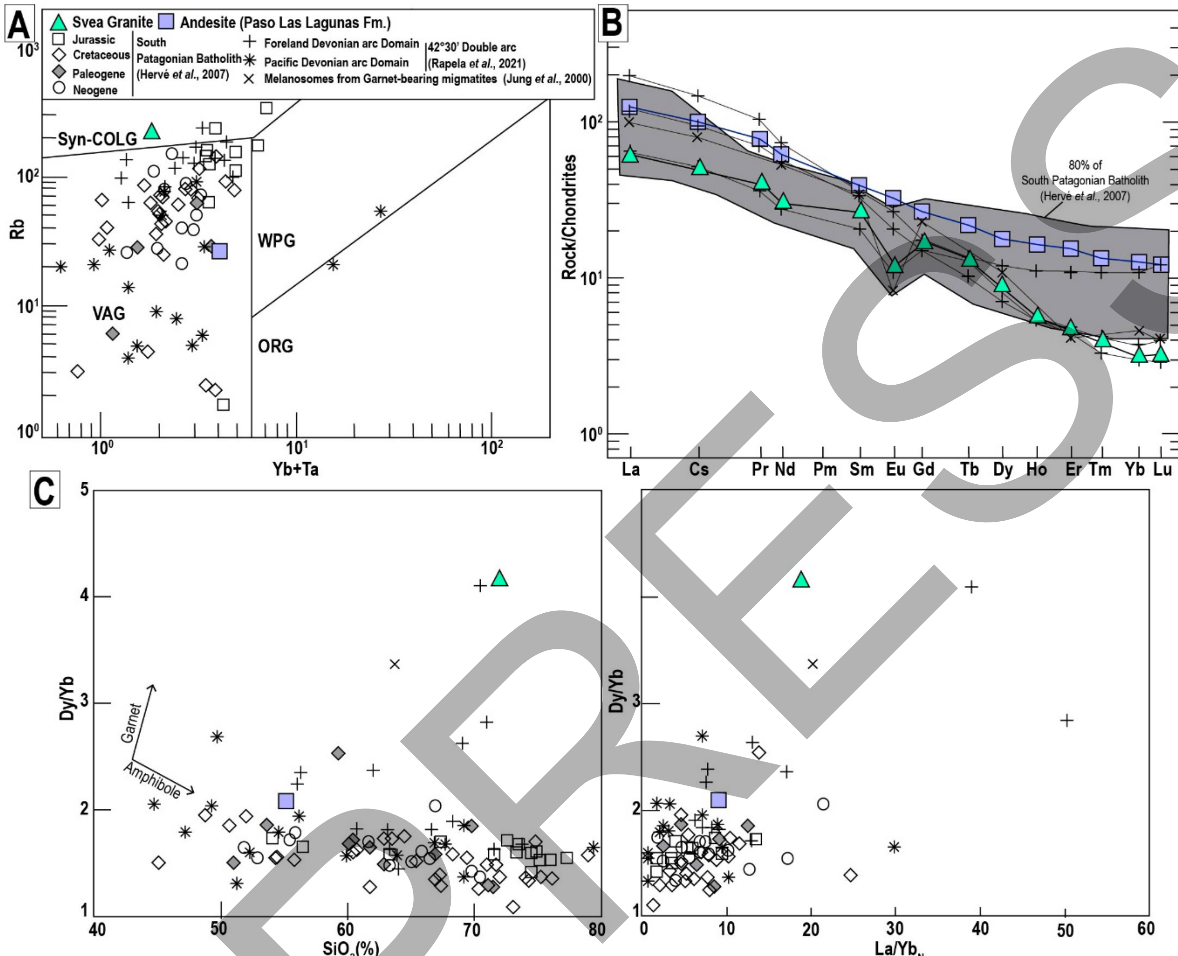

Fig. 6. A. Rb vs. Yb+Ta tectonic discrimination diagram (Pearce *et al.*, 1984); WPG: within-plate granites; VAG: volcanic arc granites; ORG: ocean ridge granites; syn-COLG: syn-collisional granites. **B.** Chondrite-normalized REE diagram (Sun and McDonough, 1989) for Svea Granite and hornblende andesite (Paso Las Lagunas Formation); shaded area represents the range encompassing 80% of the samples from the South Patagonian Batholith by Hervé *et al.* (2007b). **C.** Dy/Yb vs. SiO_2 diagram showing the affinity of the Svea Granite for fractionation of a garnet-bearing source, plotting outside the Mesozoic arc trend. The andesite of the Paso Las Lagunas Formation, by contrast, falls within the arc trend. **D.** Dy/Yb vs. La/Yb_N diagram showing the depleted heavy-REE behavior of the Svea Granite, consistent with fractionation of a garnet-bearing source.

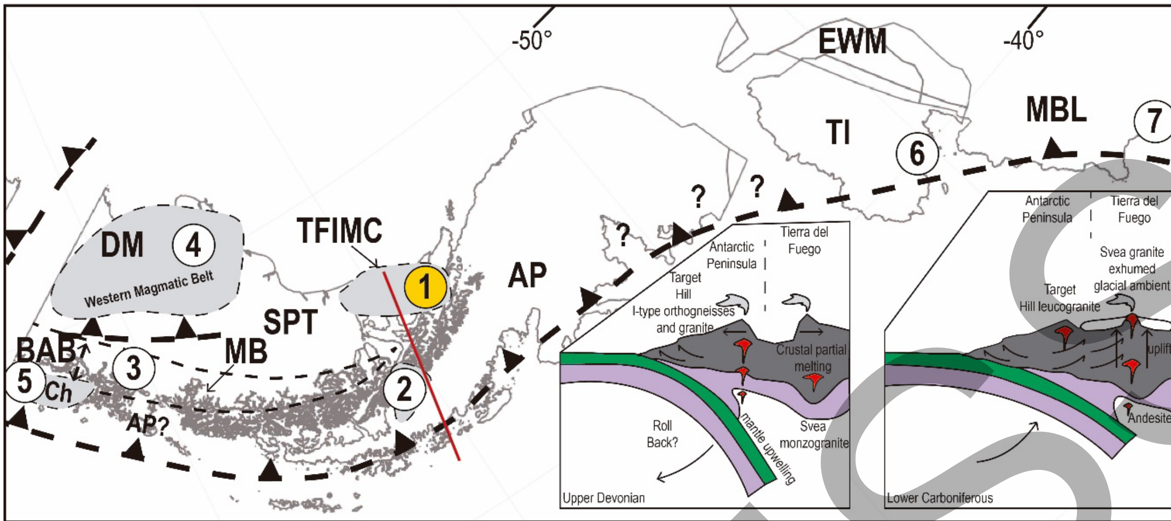

Fig. 7. Kinematic (GPlates) reconstruction for the Gondwana margin during the Late Devonian-early Carboniferous, illustrating a subduction zone in the southwestern margin of Gondwana with an associated marginal basin (MB) or back-arc basin (BAB). Numbers indicate occurrences of magmatism and/or sedimentary sequences (after Elliot *et al.*, 2015; Rojo *et al.*, 2021; Riley *et al.*, 2023; Rapela *et al.*, 2024). Global plate reconstructions after Merdith *et al.* (2021). TFIMC: Tierra del Fuego Igneous Metamorphic Complex; SPT: South Patagonian Terrane; AP: Antarctic Peninsula; TI: Thurston Island; EWM: Ellsworth-Whitmore Mountains; MBL: Marie Byrd Land. 1: Svea Granite and Paso Las Lagunas Formation; 2: Target Hill granitic orthogneiss; 3: Leones Pluton, Bahía de la Lancha Formation and serpentinites; 4: Deseado massif (DM); 5: Chaitenia Island arc (Ch: Hervé *et al.*, 2018); 6: Morgan Inlet granodiorite gneiss; 7: Fosdick Mountains granitoids. Insets illustrate the geodynamic setting and magmatism of Tierra del Fuego and the Antarctic Peninsula, modified from Pankhurst (1990) and Millar *et al.* (2001).

Table 1. Summary of U-Pb zircon and $^{40}Ar/^{39}Ar$ ages.

Sample	UTM Coordinates		Unit	Lithology	Mineral	Age (Ma)	Method	Laboratoy
	Easting (m)	Northing (m)						
MM160223-02d	517909	3944863	Paso Las Lagunas Fm.	Paraconglomerate	Zircon	345±2 (3)	U-Pb	ZirChron LLC
MM070322-03Dd	490275	3956464	Paso Las Lagunas Fm.	Intrasparite	Zircon	342±2 (3)	U-Pb	Sernageomin
MM060321-2Bd	517030	3947251	Paso Las Lagunas Fm.	Sandstone clast into pebbly shale	Zircon	340±2 (3)	U-Pb	Sernageomin
MM100320-4Ad	511861	3950723	Paso Las Lagunas Fm.	Andesite	Zircon	350±2 (2)	U-Pb	Sernageomin
MM100320-1Ad	515441	3946760	Paso Las Lagunas Fm.	Fine-grained wake and mudstone	Zircon	364±3 (3)	U-Pb	Sernageomin
TFDQ-14d	512078	3950495	Paso Las Lagunas Fm.	Pebbly shale	Zircon	375±2 (3)	U-Pb	Sernageomin
TFDQ-19d	515375	3946848	Paso Las Lagunas Fm.	Quartz sandstone	Zircon	372±2 (3)	U-Pb	Sernageomin
MM130221-4d	519487	3947644	Paso Las Lagunas Fm.	Arkosic sandstone	Zircon	377±2 (3)	U-Pb	Sernageomin
MM091222-02d	514859	3947654	Paso Las Lagunas Fm.	Arkosic sandstone	Zircon	376±2 (3)	U-Pb	ZirChron LLC
MM100320-1Dd	515163	3946958	Svea Granite	Monzogranite	Muscovite	363,4±1,3 (1)	$^{40}Ar/^{39}Ar$	Sernageomin
MM100320-1Dd	515163	3946958	Svea Granite	Monzogranite	Zircon	375±2 (2)	U-Pb	Sernageomin
MM091222-03d	514807	3947539	Svea Granite	Monzogranite	Zircon	375±1 (2)	U-Pb	ZirChron LLC
MM100320-1Cd	515157	3946615	Svea Granite	Gneiss	Muscovite	345,9±1,5 (1)	$^{40}Ar/^{39}Ar$	Sernageomin
MM100320-1Cd	515157	3946615	Svea Granite	Gneiss	Zircon	387±3 (2)	U-Pb	Sernageomin